Archives of Photogrammetry, Cartography and Remote Sensing, vol. 37, pp. 11-20
ISSN 2083-2214, eISSN 2391-9477
DOI: http://doi.org/10.14681/apcrs-2025-001

RESEARCH ARTICLE

PYTHON PIPELINE FOR PROCESSING APOLLO 17 TOPOGRAPHIC CAMERA IMAGERY

Adrian Macek

Doctoral School, Warsaw University of Technology, Poland

KEY WORDS: Photogrammetry, Bundle Adjustment, Apollo, Python

ABSTRACT: This study presents a semi-automated photogrammetric workflow for processing archival lunar imagery acquired by the Metric Camera aboard the Apollo missions Scientific Instrument Module (SIM) Bay. The proposed method, implemented in Python, includes tie point extraction, a custom bundle adjustment procedure leveraging the Schur complement and compressed Jacobian structure, and orthorectification of images. Ground Control Points and Check Points were established using crater centroids measured from LOLA-derived elevation data. The results demonstrate the potential of modern photogrammetric techniques in the processing of historical lunar data in Python.

1. INTRODUCTION

The Apollo 17 mission launched on December 7, 1972, marking the last chapter of NASA's legendary Apollo program. Among the various experiments carried out during the mission were studies of the Moon's gravity and seismic activity. However, one of the most significant scientific goals of the Apollo 17 was to gather detailed photographic and mapping data of the lunar surface (NASA, 2017a). To achieve this, the spacecraft was equipped with the SIM Bay (Scientific Instrument Module Bay), a compartment housing highly specialized photogrammetry instruments. At its core were two key systems: a panoramic camera and the Lunar Mapping Camera system the latter comprising a topographic camera, a star tracker, and a laser altimeter. Together, these systems were designed to produce accurate maps and models of the Moon. This work presents an attempt to develop a semi-automated image processing pipeline in Python for photographs taken by the Metric Camera, which was part of the SIM Bay instrumentation. To achieve this, a custom solution was built entirely from scratch. Including a bundle adjustment solution, incorporating modern state-of-the-art techniques.

2. FAIRCHILD LUNAR MAPPING CAMERA CHARACTERISTICS

The Fairchild Lunar Mapping Camera, used during NASA's Apollo missions 15 through 17, was a highly advanced imaging system designed to capture high-resolution photographs

of the Moon from orbit. Installed in the Scientific Instrument Module (SIM) bay of the Apollo Service Module, it integrated three key components: a metric (terrain) camera, a stellar camera, and a laser altimeter. The metric camera featured a 3-inch (76 mm) f/4.5 lens and captured 4.5 x 4.5-inch images on 5-inch-wide film, offering a 74° by 74° field of view (Figure 1). To ensure image quality, it included automatic exposure control, forward motion compensation, and a glass plate that held the film flat during exposure. The stellar camera, with a similar 3-inch lens and a wider f/2.8 aperture, simultaneously recorded star fields on 35-mm film within a 24° cone, allowing precise determination of the spacecraft's orientation. Meanwhile, the laser altimeter measured the spacecraft's altitude above the lunar surface, synchronizing with the metric camera to provide elevation data for each image (NASA, 2017b). By combining imagery from the metric and stellar cameras with altitude data and spacecraft navigation information, the system enabled the creation of highly accurate lunar maps.

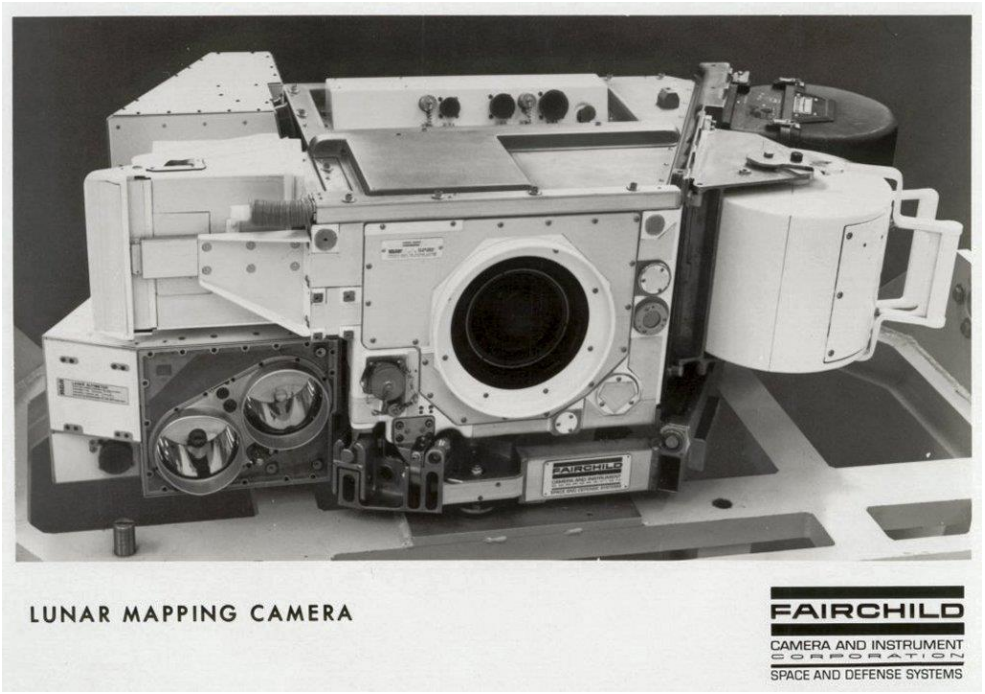


Fig. 1. Farichild Lunar Mapping Camera (NASA / FAIRCHILD)

A calibration metric is available for the camera, containing the coordinates of the fiducial marks. These coordinates were later used to compute the transformation parameters between the pixel coordinate system and the fiducial coordinate system (Table 1).

Tab. 1. Coordinates of LMC metric camera fiducials (NASA, 1971)

Fiducial	x	y
A	-60.614	0.0
B	60.627	0.0
C	0.010	-60.482
D	-0.011	60.439
A’	-60.555	30.796
B’	60.475	-30.754
C’	-30.662	-60.566
D’	30.678	60.580

There are also intrinsic calibration parameters available, including focal length, principal point, and radial and tangential distortion coefficients. These were applied during image rectification and modeling:

Tab. 2. Distortion provided in camera calibration summary (NASA, 1971)

Parameter	Value
f	75.842
Principal Point	-0.005,-0.007
K1	-0.0000013002628
K2	0.00000000053903721
K3	-0.000000000000054031164
J1	0.00000085729357
J2	-0.00000000017887586
theta	3.1067218

The distortion models applied in this study are based on the analytical equations included in the camera calibration report (NASA, 1971), which were also utilized during the original lunar image processing in the 1970s, according to formula 1

.

$$dx = x(K_1 r^2 + K_2 r^4 + K_3 r^6) - (J_1 r^2 + J_2 r^4)\left[\left(1 + \frac{2x^2}{r^2}\right) sin\theta - \frac{2xy}{r^2} cos\theta\right]$$
$$dy = y(K_1 r^2 + K_2 r^4 + K_3 r^6) + (J_1 r^2 + J_2 r^4)\left[\left(1 + \frac{2y^2}{r^2}\right) cos\theta - \frac{2xy}{r^2} sin\theta\right] \quad (1)$$

3. DATA PREPARATION AND PROCESSING

The processing pipeline consists of several stages, shown in Figure 2. In the first stage, fiducial markers are manually measured on the images, and their coordinates are entered. This enables the transformation between the pixel coordinate system and the fiducial coordinate system, which is essential for achieving the required accuracy in later stages. In the next step, tie points are automatically detected using the Agisoft API. The Agisoft API was chosen because the OpenCV library does not support an even distribution of tie points, especially in Von Gruber regions. Ground Control Points (GCPs) and Check Points are then identified semi-automatically using a Digital Elevation Model (DEM) as a reference. These measured points, along with the LCM trajectory data, are passed into a custom bundle adjustment implementation that leverages a Levenberg–Marquardt optimization and a Reduced Bundle System strategy. In the final stage, the refined camera positions and the DEM are used to orthorectify and stitch the images.

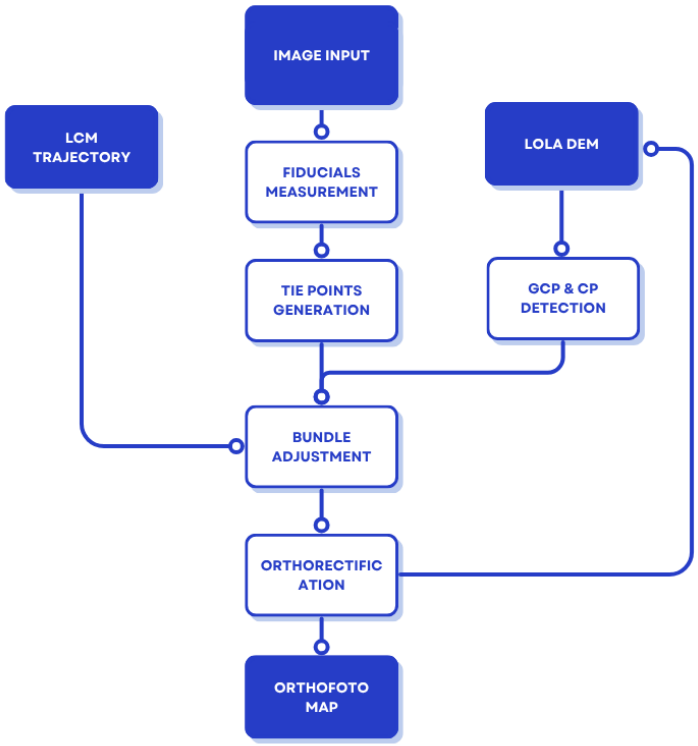


Fig. 2. Created Python processing pipeline

3.1. Transformation between pixel and fiducial coordinate systems

Using the fiducial mark coordinates from the camera calibration report and their measured pixel coordinates on the images, the transformation parameters between the image coordinate system and the fiducial coordinate system were computed. An affine transformation of the following form (Luhmann *et al.*, 2006) was used below:

$$\begin{bmatrix} X \\ Y \end{bmatrix} = \begin{bmatrix} a_1 a_2 \\ b_1 b_2 \end{bmatrix} \begin{bmatrix} x \\ y \end{bmatrix} + \begin{bmatrix} a_0 \\ b_0 \end{bmatrix} \tag{2}$$

The transformation parameters a_0, a_1, a_2, b_0, b_1 and b_2 were calculated separately for each image by solving a system of equations using the least squares method.

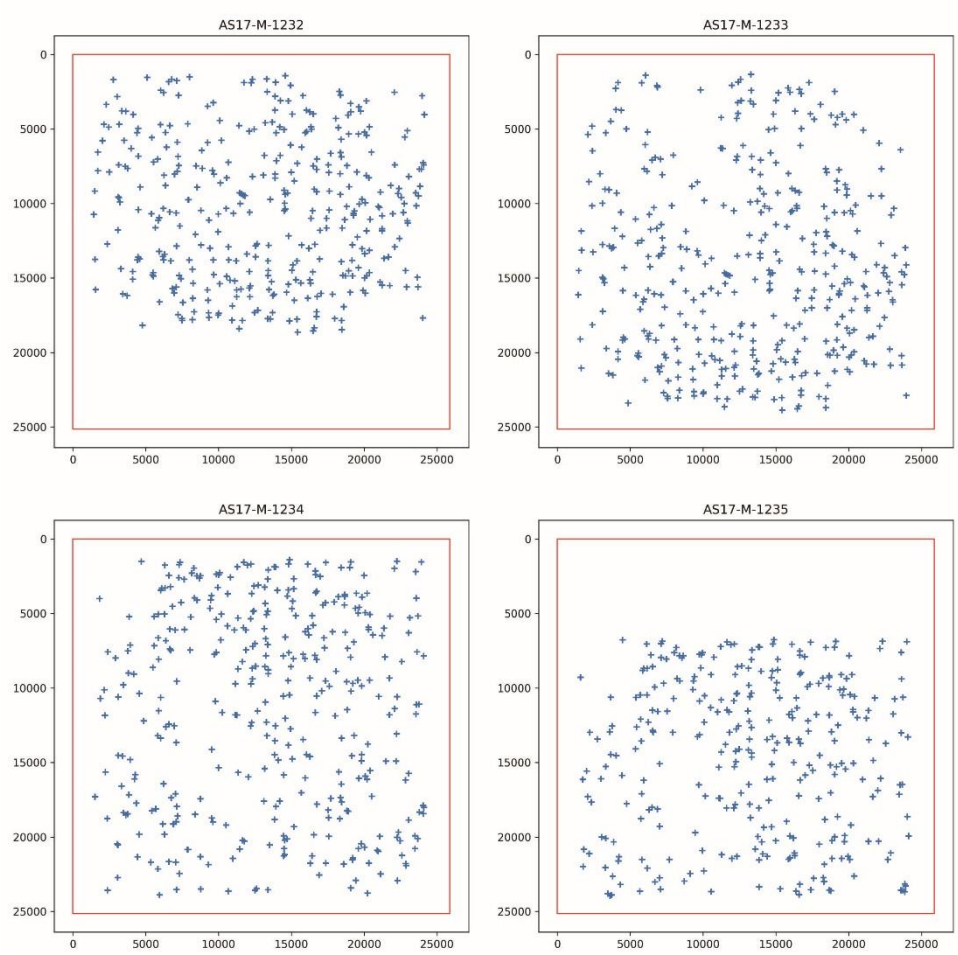


Fig. 3. Tie-Points distribution

3.2. Measurement of Tie Points and GCP

The Agisoft Metashape API was used to automatically measure and export tie points, with around 400 points detected per image which was shown in Figure 3. These tie point coordinates were then transformed into the fiducial coordinate system using previously computed affine transformation parameters. The network of Ground Control Points (GCPs) and Control Points was established based on crater locations, as craters are among the few easily identifiable features on the lunar surface. The coordinates of the GCPs and Control Points were derived from the LOLA/SELENE Digital Elevation Model (LRO LOLA and SELENE/Kaguya Team, 2015) by fitting ellipses to the crater rims and calculating their centroids. In total, the study area included 22 GCPs and 4 Control Points.

4. BUNDLE ADJUSTMENT

To determine the camera position for each exposure, a custom bundle adjustment was implemented using the Schur complement and a Reduced Bundle System within the Levenberg-Marquardt algorithm (*Triggs et al., 2000; Lourakis & Argyros, 2009; Chen et al., 2019*). The input to the bundle adjustment included initial estimates of camera positions, ground control points (GCPs), control points, and tie points. The initial values for the tie points were computed using photogrammetric space intersection (triangulation). All coordinates were expressed in cartesian Moon-Centered, Moon-Fixed reference frame.

Bundle adjustment can be expressed in a general form as:

$$\left(J^T J + \lambda diag(J^T J)\right)\delta x = -J^T r \tag{3}$$

The above equation can be reduced to the form of the Reduced Bundle System.

$$\begin{bmatrix} U & W \\ W^T & V \end{bmatrix} \cdot \begin{bmatrix} \delta c \\ \delta p \end{bmatrix} = \begin{bmatrix} r_c \\ r_p \end{bmatrix} \tag{4}$$

Accordingly, approximate Hessian for RBD can be expressed in the following generalized form

$$J^T J = \begin{bmatrix} U_1 & 0 & \dots & 0 & W_{11} & W_{21} & \dots & W_{N1} \\ 0 & U_2 & \dots & 0 & W_{12} & W_{22} & \dots & W_{N2} \\ \vdots & \vdots & \ddots & \vdots & \vdots & \vdots & \ddots & \vdots \\ 0 & 0 & \dots & U_n & W_{1n} & W_{2n} & \dots & W_{Nn} \\ W_{11}^T & W_{12}^T & \dots & W_{1n}^T & V_1 & 0 & \dots & 0 \\ W_{21}^T & W_{22}^T & \dots & W_{2n}^T & 0 & V_2 & \dots & 0 \\ \vdots & \vdots & \ddots & \vdots & \vdots & \vdots & \ddots & \vdots \\ W_{N1}^T & W_{N2}^T & \dots & W_{Nn}^T & 0 & 0 & \dots & V_N \end{bmatrix} \tag{5}$$

with its elements evaluated using the following equations.

$$\begin{gathered} U_j = \sum_{i \in I_j} A_{ij}^T A_{ij} + \lambda \cdot diag\left(\sum_{i \in I_j} A_{ij}^T A_{ij}\right) \\ V_i = \sum_{j \in J_i} B_{ij}^T B_{ij} + \lambda \cdot diag\left(\sum_{j \in J_i} B_{ij}^T B_{ij}\right) \\ W_{ij} = A_{ij}^T B_{ij} \end{gathered} \tag{6}$$

where λdiag() serve as the regularization component of Levenberg–Marquardt and A and B denote the partial derivatives matrices corresponding to the camera's interior orientation parameters and 3D point positions, respectively

$$A_{ij} = \begin{bmatrix} \frac{\partial x_{ij}}{\partial w_{xj}} & \frac{\partial x_{ij}}{\partial w_{yj}} & \frac{\partial x_{ij}}{\partial w_{zj}} & \frac{\partial x_{ij}}{\partial t_{xj}} & \frac{\partial x_{ij}}{\partial t_{yj}} & \frac{\partial x_{ij}}{\partial t_{zj}} \\ \frac{\partial y_{ij}}{\partial w_{xj}} & \frac{\partial y_{ij}}{\partial w_{yj}} & \frac{\partial y_{ij}}{\partial w_{zj}} & \frac{\partial y_{ij}}{\partial t_{xj}} & \frac{\partial y_{ij}}{\partial t_{yj}} & \frac{\partial y_{ij}}{\partial t_{zj}} \end{bmatrix} \tag{7}$$

and

$$B_{ij} = \begin{bmatrix} \frac{\partial x_{ij}}{\partial X_i} & \frac{\partial x_{ij}}{\partial Y_i} & \frac{\partial x_{ij}}{\partial Z_i} \\ \frac{\partial y_{ij}}{\partial X_i} & \frac{\partial y_{ij}}{\partial Y_i} & \frac{\partial y_{ij}}{\partial Z_i} \end{bmatrix} \tag{8}$$

Subsequently, the adjustments to the camera positions δc are computed separately as part of the least squares adjustment.

$$U - WV^{-1}W^T \delta c = r_c - WV^{-1} r_p \tag{9}$$

And for the 3D points, by substituting δc into the following expression:

$$\delta p = V^{-1}\left(r_p - W^T \delta c\right) \tag{10}$$

5. RESULTS

The bundle adjustment process yielded generally satisfactory results, though with some notable limitations. The mean reprojection error after adjustment was around 25μ, suggesting the presence of residual geometric discrepancies in the model consistency.

Tab. 3. Final RMSE for each image

Image ID	RMS [μ]
AS17-M-1232	17.7
AS17-M-1233	34.3
AS17-M-1234	16.6
AS17-M-1235	31.1

Based on the adjusted parameters, an orthophotomap was generated (Figure 4). The resulting orthophoto had a ground sampling distance of 20 meters. While overall crater placement and image alignment were reasonable, some local geometric inconsistencies remain visible, particularly in areas of limited tie point coverage or steep topography. Minor color mismatches are also present along some images, likely due to varying illumination conditions and differences in film exposure across the image set.

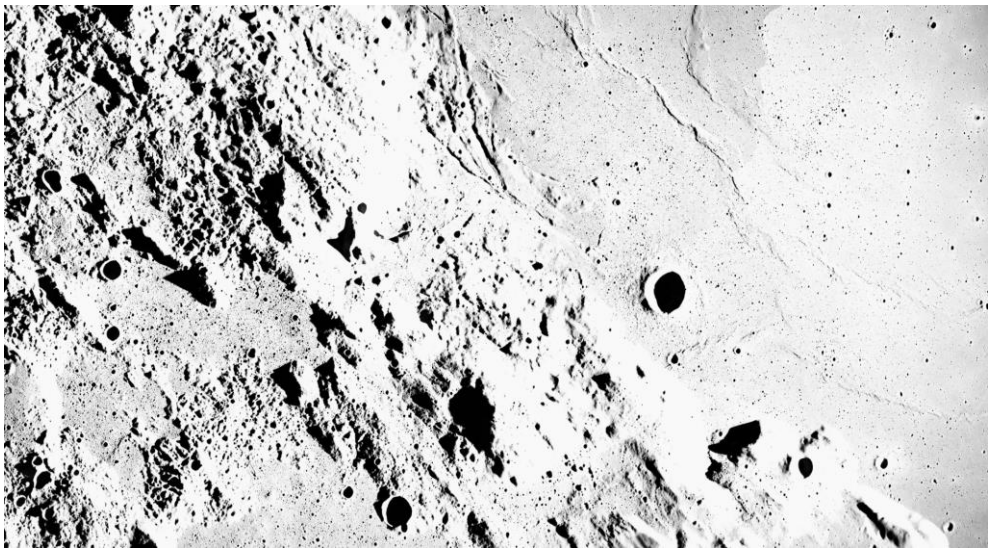


Fig. 4. The orthophotomap generated by mosaicking rectified images obtained

Despite these issues, the results confirm that the developed Python workflow is capable of producing usable cartographic outputs. However, to improve the geometric accuracy and consistency of future results, a denser and more evenly distributed tie point network would be beneficial. Additionally, more robust outlier detection and rejection mechanisms particularly during feature matching and initial triangulation could significantly reduce local distortions and improve the reliability of the bundle adjustment.

REFERENCES

Chen, Y., Chen, Y., & Wang, G. 2019. Bundle adjustment revisited. arXiv. Retrieved from https://arxiv.org/abs/1912.03858 doi: 10.48550/ARXIV.1912.03858

Lourakis, M. I. A., & Argyros, A. A. 2009. Sba: A software package for generic sparse bundle adjustment. ACM Trans. Math. Softw., 36(1). Retrieved from https://doi.org/10.1145/1486525.1486527 doi: 10.1145/1486525.1486527

Luhmann, T., Robson, S., Kyle, S. A., & Boehm, J. 2006. Close range photogrammetry: Principles, techniques and applications. Whittles Publishing.

Lunar Reconnaissance Orbiter LOLA Team and SELENE/Kaguya Team. (2015, February 4). Moon lro lola – selene kaguya tc dem merge 60n–60s 59m (sldem2015). Data set, USGS Astrogeology Science Center. Retrieved from https://astrogeology.usgs.gov/search/map/moon_lro_lola_selene_kaguya_tc_dem_merge_60n60s_59m

NASA. 1971. Camera calibration summary.
https://apollo.im-ldi.com/RESOURCES/Appendix_A.pdf . (Accessed: June 6, 2025)

NASA. 2017a. Apollo 17 photographic task requirements.
https://www.nasa.gov/history/afj/simbaycam/a17-photo-task.html. (Accessed:June 6, 2025)

NASA. 2017b. Fairchild lunar mapping camera.
https://www.nasa.gov/history/afj/simbaycam/fairchild-lunar-mapping-camera.html
(Accessed: June 6, 2025)

Triggs, B., Mclauchlan, P., Hartley, R., & Fitzgibbon, A. 2000. Bundle adjustment – a modern synthesis. ICCV '99 Proceedings of the International Workshop on Vision

ZAUTOMATYZOWANY PROCES DO PRZETWARZANIA ZDJĘĆ Z MISJI APOLLO 17 W PYTHON

SŁOWA KLUCZOWE: Fotogrametria, Bundle Adjustment, Apollo, Python

Streszczenie

Niniejsza publikacja przedstawia półautomatyczny proces fotogrametryczny do przetwarzania archiwalnych zdjęć Księżyca, wykonanych przez kamerę metryczną znajdującą się w module naukowym (SIM) misji Apollo. Zaproponowana metoda, zaimplementowana w języku Python, obejmuje ekstrakcję punktów wiążących, napisany od podstaw moduł aerotriangulacji wykorzystujący dopełnienie Schura oraz strukturę skompresowanego jakobianu, a także ortorektyfikację obrazów. Punkty osnowy i punkty kontrolne zostały ustalone na podstawie środków kraterów zmierzonych z wykorzystaniem danych wysokościowych pochodzących z misji LOLA. Wyniki pokazują potencjał nowoczesnych technik fotogrametrycznych w przetwarzaniu historycznych danych księżycowych w środowisku Python.

Details of authors:

Mgr inż. Adrian Macek
e-mail: adrian.macek@pm.me

Submitted 30.06.2025
Accepted 1.12.2025